STP 1597, 2018 / available online at www.astm.org / doi: 10.1520/STP159720160095

Arthur T. Motta[1]

Mechanistic Understanding of Zirconium Alloy Fuel Cladding Performance

Citation

Motta, A. T., "Mechanistic Understanding of Zirconium Alloy Fuel Cladding Performance," *Zirconium in the Nuclear Industry: 18th International Symposium*, *ASTM STP1597*, R. J. Comstock and A. T. Motta, Eds., ASTM International, West Conshohocken, PA, 2018, pp. 19–51, http://dx.doi.org/10.1520/STP159720160095[2]

ABSTRACT

A review is presented of work performed in our group over the years in the areas of radiation damage, corrosion, hydrogen pickup, hydriding, and the mechanical behavior of zirconium alloy nuclear fuel cladding with the goal of developing a greater mechanistic understanding of cladding performance in service.

Keywords

zirconium, cladding, fuel performance, radiation damage, corrosion, hydriding, hydrogen pickup, mechanical properties

Introduction

It is a great honor to have been selected as the 2014 recipient of the ASTM William J. Kroll Medal. I thank the selection committee and my nominators for this very special recognition. This award has a unique significance in my career for many reasons. In the first place, this is the community of scientists that best knows my work and there is no higher distinction to a scientist than the recognition of one's peers. Second, it is a very select group of people that have been given this distinction previously, from the first two awardees, Admiral Rickover and Brian Cox, through many

Manuscript received April 25, 2016; accepted for publication August 16, 2016.

[1]Pennsylvania State University, Dept. of Mechanical and Nuclear Engineering, University Park, PA, 16802

[2]ASTM 18th International Symposium on *Zirconium in the Nuclear Industry* on May 15–19, 2016 in Hilton Head, SC.

others, some of whom I have worked with and known over the years and who made seminal contributions to the field, such as Rick Holt, Ron Adamson, George Sabol, and Clément Lemaignan. I have been fortunate enough to have worked with and known personally many of the other awardees on the list, and coming to this meeting every three years has been a crucial factor in my development as a scientist. Finally, this award provides an opportunity to honor and share the moment with many of my former colleagues, students, and collaborators. Working alongside students and colleagues to discover new phenomena by asking questions, planning and conducting experiments, analyzing data, and developing and testing models has truly been the greatest source of satisfaction in my professional career.

The citation in the award is for contributions to zirconium metallurgy in the areas of oxidation, hydriding, deformation, and radiation damage. The breadth of subjects studied is a good indicator of the approach of a university professor who rather than specializing in one area tries peripatetically to study all relevant phenomena. Through working with others who have taught me immensely I have been fortunate to be able to make contributions in all these areas. However, whatever work I present herein has been for the most part performed by my students and enormously enhanced by the contributions of many colleagues, too numerous to cite in their entirety. I do want to recognize two great colleagues with whom I have collaborated closely for over 15 years: Bob Comstock, in the domain of corrosion and hydrogen pickup, and Don Koss, on the study of the mechanical properties of hydrided Zircaloy.

In the early days of Rickover, Lustman, Kerze, Kass, and coworkers who were developing zirconium alloys to be used in the Nuclear Navy, scientific and technological progress was fast [1]. An enormous amount of work was done in those days to create a workable alloy that could provide a stable structural metal for use in nuclear reactors [2–4]. By necessity, this approach had to be focused on the engineering aspects of alloy development so that many of the questions as to why did a particular metallurgical recipe work well were left for later.

Taking advantage of novel and advanced characterization techniques, we have been able, over the years and after the fact, to reconstruct the role of alloying elements in material behavior (corrosion, hydrogen pickup, mechanical properties) and to explore the behavior of these alloys in more demanding regimes (i.e., more severe duty: higher temperature, longer burnups, aggressive chemistry) so as to generate a deeper understanding of material behavior. It is a truism that it is not possible to generate experimental databases extensive enough to cover all the operational conditions of interest. This necessitates the development of an accurate understanding of the underlying physics and of robust models that can interpolate and predict behavior within the database but also extrapolate to regions outside it. In addition, since those early times, many problems have been solved and new problems have arisen to occupy us. Addressing these issues in a fundamental and mechanistic manner has been the focus of my career. I review some of this work in this paper.

Radiation Damage

Because zirconium fuel cladding is under a neutron flux when in a nuclear reactor, its microstructure changes significantly [5–7]. During neutron irradiation, atoms are displaced from their lattice positions creating point defects that can react with one another to form clusters (causing radiation hardening and affecting phenomena such as creep and growth). As these processes occur, the material microstructure and microchemistry (which in the as-fabricated state had been optimized to improve cladding properties) evolve, causing the material to exhibit different—usually worse—properties after irradiation.

My doctoral thesis work at the University of California, Berkeley under Don Olander's supervision and funded by Albert Machiels at the Electric Power Research Institute (EPRI) was initially focused on investigating alloying element redistribution in Zircaloy-4 using charged-particle irradiation (ions). In this project we collaborated with the GE-Vallecitos group of Ron Adamson and Walter Yang, and in 1985 they came to us with an interesting observation that was also reported by Malcolm Griffiths and Ross Gilbert [8,9]. During neutron irradiation the $Zr(Cr,Fe)_2$ Laves-phase precipitates underwent a crystal-to-amorphous transformation (amorphization) that was associated with a loss of iron from the precipitates into the matrix and eventual precipitate dissolution.

Interestingly, the amorphization process in these precipitates occurred through the formation of a "duplex" structure with an amorphous layer on the outside that traveled inward as the fluence increased. This amorphous layer was depleted in iron, although the chromium content hardly changed. Measurements of the amorphous-layer thickness as a function of fluence showed that the layer advanced inward at a constant speed of 10 nm/10^{25} n/m^2 ($E > 1$ MeV) [10]. We then refocused the thesis work to study the irradiation-induced amorphization of precipitates in Zircaloy. After many attempts to induce precipitate amorphization using ion irradiation (the dose was not high enough and it was difficult to keep the irradiation temperature down to favor amorphization), Gareth Thomas of the Materials Science Department suggested we use electron irradiation to induce amorphization in the Kratos HVEM at Lawrence Berkeley Laboratory. This idea initially appeared counterintuitive as the damage from electrons is much less concentrated than radiation damage from ions or neutrons (much less energy can be imparted to the struck atom in a given collision). In particular, for the most part only single point defects are created and no displacement cascades are present. In addition, the displacement cross-section of high-energy electrons is much lower than that of other charged particles [11]. These factors are, however, compensated by the fact that a focused electron beam generates a flux about six orders of magnitude higher than that of a typical ion accelerator. The initial electron irradiation experiment in the Kratos, conducted at room temperature, resulted in no amorphization, but as soon as the temperature was lowered to liquid nitrogen, amorphization occurred in a couple of minutes. **Fig. 1** shows a bright-field electron micrograph showing precipitates in Zircaloy before and after electron irradiation.

FIG. 1 Amorphization of intermetallic precipitates in Zircaloy under electron irradiation. *a*, *b*, and *c* are amorphous while *d* is still crystalline.

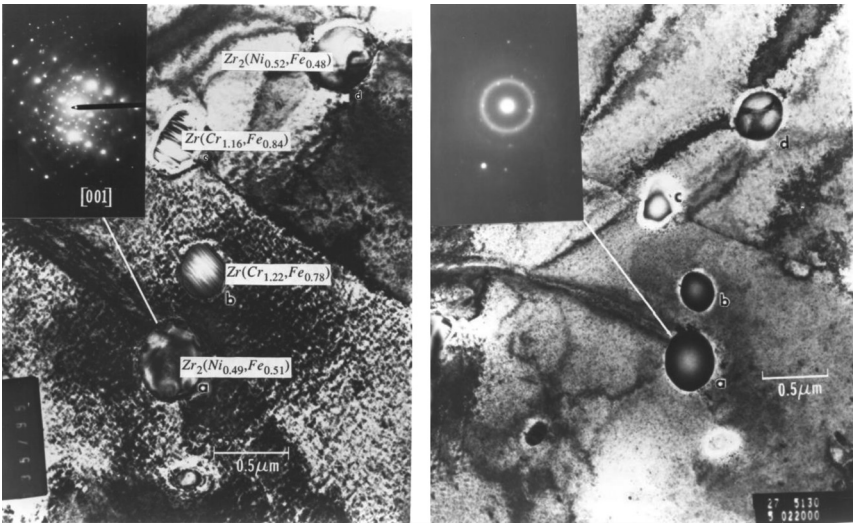

By inducing amorphization in the microscope it was possible to determine the kinetics of amorphization in situ as a function of irradiation temperature from cryogenic temperatures (77 K) to room temperature. The dose to amorphization could be plotted against irradiation temperature, and it was found that the critical temperature for amorphization was close to room temperature [12].

Fig. 2 shows schematically the behavior of the the dose to amorphization under different types of irradiation [13]. It is clear that the critical temperature for amorphization under cascade-producing irradiation is much higher than that under electron irradiation.

We then developed a model of amorphization under electron irradiation that accounted for the amorphization kinetics by calculating the increase in the free energy of the precipitate after irradiation from chemical disordering and lattice defects [14]. Fig. 3 shows the different contributions of chemical disordering and point defect accumulation to reach the amorphization level as calculated by the model. According to this model the dose to amorphization D (in dpa) was given as

$$D.\sqrt{k} = B\ \exp(-2E_i^m/k_BT) \tag{1}$$

where:

D = dose to amorphization (dpa),
k = damage rate,
E_i^m = interstitial migration energy, k_B = Boltzmann's constant
T = irradiation temperature, and
B = constant.

FIG. 2 Schematic dose to amorphization versus irradiation temperature for $Zr(Cr,Fe)_2$ precipitates in Zircaloy under electron, ion, and neutron irradiation.

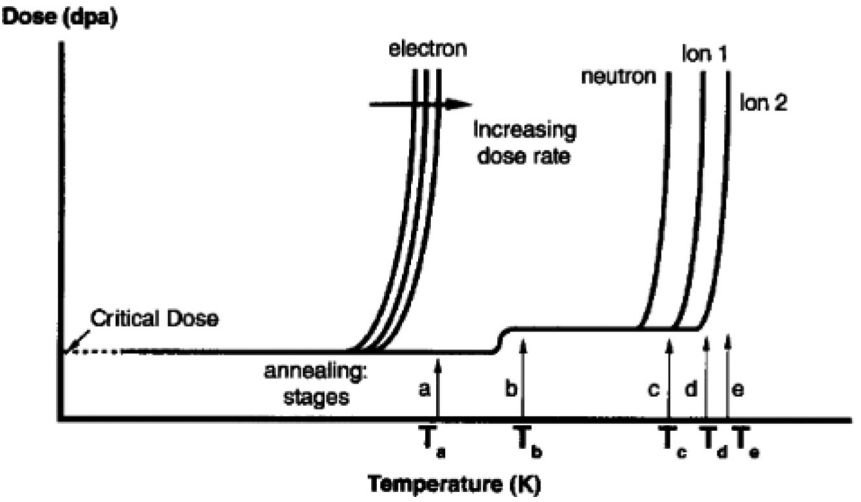

FIG. 3 Free-energy change during electron irradiation versus irradiation dose.

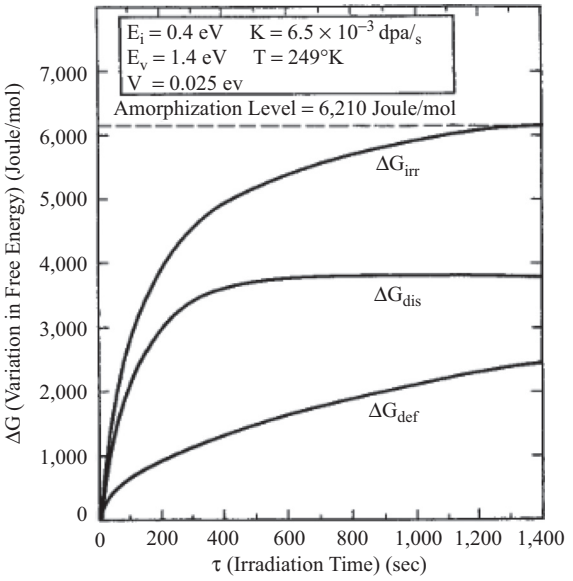

The model predicted a slight effect that was later verified [15,16] of increasing dose rate on increasing the critical temperature for amorphization. However, the specific amorphization mechanism under neutron irradiation was clearly different from that under electron irradiation. In particular, it exhibited the duplex structure mentioned previously with an amorphous layer that started at the precipitate/matrix interface (**Fig. 4a**) and slowly advanced into the core of the precipitate at an approximately constant rate of 10 nm/10^{25} n/m^2. The amorphous layer was also depleted in iron but not in chromium (**Fig. 4b**).

To rationalize this different amorphization process, a ballistic mixing model was proposed that caused amorphization induced by neutron irradiation to start near the outer surface of the precipitate where mixing could be induced by displacement cascades [17]. The chemical disordering induced by such mixing would cause the local free energy to increase above the amorphization threshold. The equation used to describe the amorphous thickness X_c was

$$X_c(t) = \frac{\mu\phi\sigma_d t}{6}\left[\frac{3\Delta C}{2\delta_c} - 1\right] \tag{2}$$

FIG. 4 (a) Bright-field electron micrograph showing amorphization of $Zr(Cr,Fe)_2$ precipitates in Zircaloy-4 under neutron irradiation; (b) iron concentration profile along the precipitate.

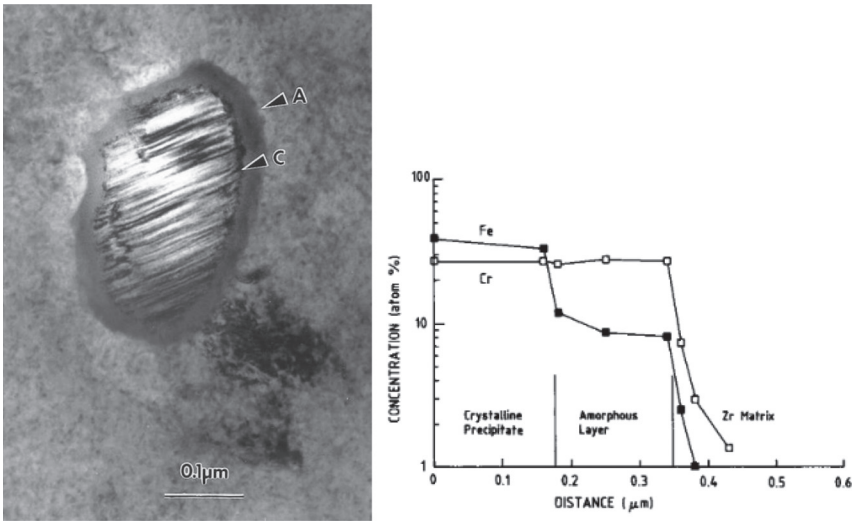

(a) (b)

where:

$\mu =$ range of ballistically expelled atoms,
$\phi =$ neutron flux,
$\sigma_d =$ displacement cross-section,
$t =$ time, and
ΔC and $\delta_c =$ differences in iron concentration between crystal and amorphous and between the region near the interface and the bulk of the precipitate, respectively.

The amorphous thickness predicted by this equation increases linearly with fluence. The calculated amorphous front advance using this model corresponds very well to the measured value. Once the precipitate is amorphous a new kinetically constrained equilibrium is then achieved in which the common tangent occurs at a lower iron concentration for the amorphous phase than for the crystalline precipitate [17]. An overall review of irradiation-induced amorphization has previously been presented [16]. The microchemical evolution of precipitates under irradiation can affect other processes. The released iron in the matrix has been correlated to the development of <c>-component loops [18], which can influence growth. More recent work has shown that the proton irradiation of Zircaloy-4 can reproduce the observed duplex structure [19]. Also, precipitates have been shown to influence corrosion [20,21], which is the topic of the next section.

Corrosion

Ever since the early days of zirconium alloy development, it was clear that alloying elements increase the stability of growing oxides in zirconium alloys. At CEA-Grenoble, a topic of early interest in the corrosion area, studied by Dominique Pêcheur in his doctoral thesis, was to determine how intermetallic precipitates were incorporated into the advancing oxide layer. Using detailed ion-milling procedures to create frontal transmission electron microscopy (TEM) samples at different depths in the oxide layer, he was able to examine precipitates in oxidized Zircaloy-4 [22,23]. **Fig. 5** shows two transmission electron micrographs (bright field and dark field) depicting a metallic precipitate in the oxide layer of Zircaloy-4. This was the first direct evidence that precipitates are incorporated into the oxide in metallic form which makes sense as the precipitates are expected to be noble with respect to the zirconium matrix. The depth to which the precipitates survived in metallic form in the oxide layer was not known. Pêcheur found that further into the layer the precipitates become first partly oxidized (chromium and zirconium oxides along with metallic iron agglomerates) and then completely oxidized.

The awareness that corrosion and hydriding are life-limiting factors in nuclear fuel cladding caused a resurgence of research support from the U.S. Department of Energy (DOE) in the late 1990s and early 2000s, as well as the incentive to collaborate with industry. In our case, this led to a very fruitful collaboration between our

FIG. 5 Metallic $Zr(Cr,Fe)_2$ Laves-phase precipitate in the oxide layer formed on Zircaloy-4.

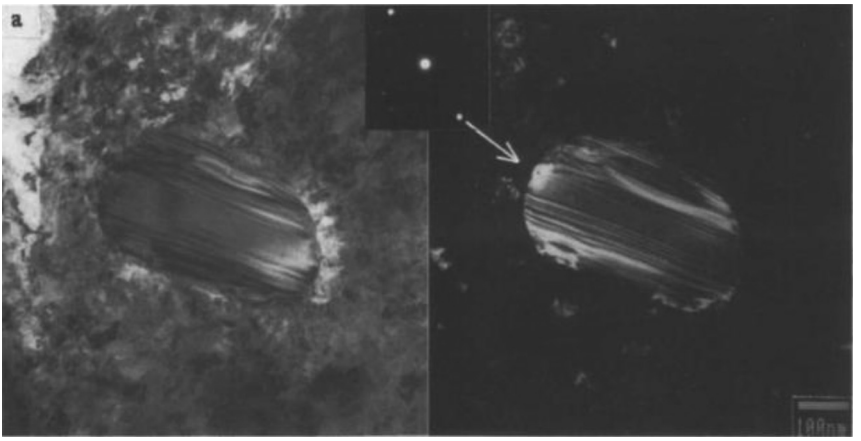

group at Penn State with Westinghouse (R. Lott, G. Sabol, J. Partezana, and R. Comstock) and other partners, including the Korea Atomic Energy Research Institute and University of Michigan, through which many new insights were achieved.

CORROSION KINETICS

The phenomenon in question is that, during service, zirconium alloy nuclear fuel cladding is exposed to high-temperature water, leading to waterside corrosion according to the overall reaction

$$Zr + 2H_2O \rightarrow ZrO_2 + 2H_2 \tag{3}$$

Some of the hydrogen generated in this reaction enters the cladding, leading to cladding embrittlement. The corrosion of zirconium alloys in a reactor environment has been studied ever since these alloys were selected for nuclear fuel cladding. At the time the collaboration with Westinghouse started, some facts were well known regarding the corrosion of zirconium alloys in 360–400°C water or steam in an autoclave, which served as a basis for our studies:

1. The oxidation of zirconium alloys occurs by oxygen ingress rather than by zirconium atom egress.
2. In alloys such as Zircaloy-4, ZIRLO™, and M5® the oxide forms a protective adherent oxide scale. No oxide dissolution is observed. As a result the weight gain is a good measure of the oxidation kinetics.
3. Upon oxidation a volume increase of 56 % occurs, essentially all of which is accommodated in the growth direction of the oxide.
4. The stable growth of the zirconium alloy oxide layer can be divided into pre- and post-transition regimes. The kinetic transition marks a point in oxide

growth where the protective oxide loses its protectiveness, such that water has easy access to the metal and the corrosion rate increases. The oxide then reforms with corrosion kinetics similar to the start of corrosion, and periodic behavior is established.

5. The specific behavior of different zirconium alloys in the same environment (corrosion rate, transition thicknesses, stable versus unstable growth, etc.) can be widely different, even though their compositional differences are quite small (less than 1 %).
6. Corrosion rate is strongly dependent on temperature but not very much dependent on the partial pressure of oxygen. The hydrogen absorbed is also relatively independent of dissolved hydrogen and comes mostly from the corrosion reaction.

As explained previously, the corrosion process can be divided into protective behavior and the rate transition. These two processes are governed by different physical phenomena [24]. In the protective regime, oxide growth is well described by a power law of the type

$$\delta = At^n \tag{4}$$

where:

δ = oxide layer thickness,
t = exposure time, and
A and n = constants.

Although this is an empirical equation, the values of A and n as well as the transition thickness are quite reproducible from sample to sample for a given alloy in a given test [25].

Detailed corrosion testing of a well-controlled set of model alloys showed results that were widely disparate depending on the alloy but quite consistent for each alloy. A representative set of these results is shown in Fig. 6.

Fig. 7 shows the values of n measured in various alloys during corrosion testing in 360°C water and 500°C supercritical water [25]. Roughly speaking, during corrosion in 360°C water, niobium-containing alloys show a value of n of approximately 0.5, whereas precipitate-forming alloys such as Zircaloy-4 and ZrFeCr model alloys show a value of n in the 0.2–0.25 range. It is also interesting to note that for all alloys studied the values of n increase during corrosion in 500°C supercritical water compared with 360°C. The different values of n will be recalled later in developing the Coupled Current Charge Compensation (C4) model.

OXIDE MICROSTRUCTURE

The microstructure of the protective oxide is quite similar among alloys. It shows a marked fiber texture that consists mostly of monoclinic oxide grains with an orientation close to $\bar{4}01$ [26,27]. Our research project hypothesized that although the oxides were very similar, the reasons for the differences in behavior could be found

FIG. 6 Corrosion weight gain for various alloys tested in autoclave in 360°C water.

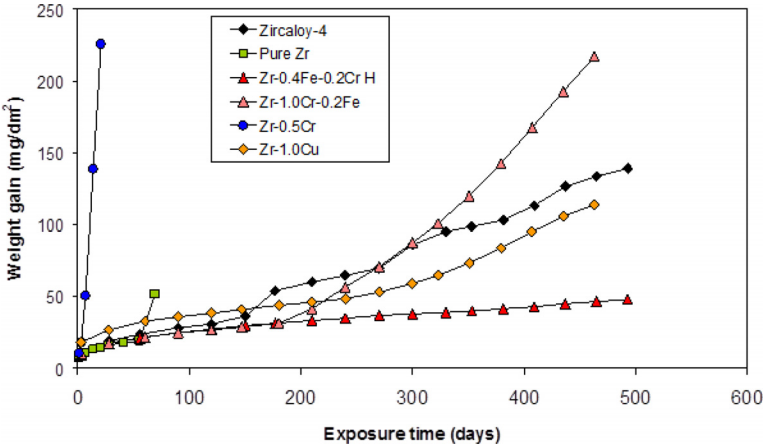

FIG. 7 Values of n for various alloys during corrosion at 360°C (bottom) and 500°C supercritical water (top) [25].

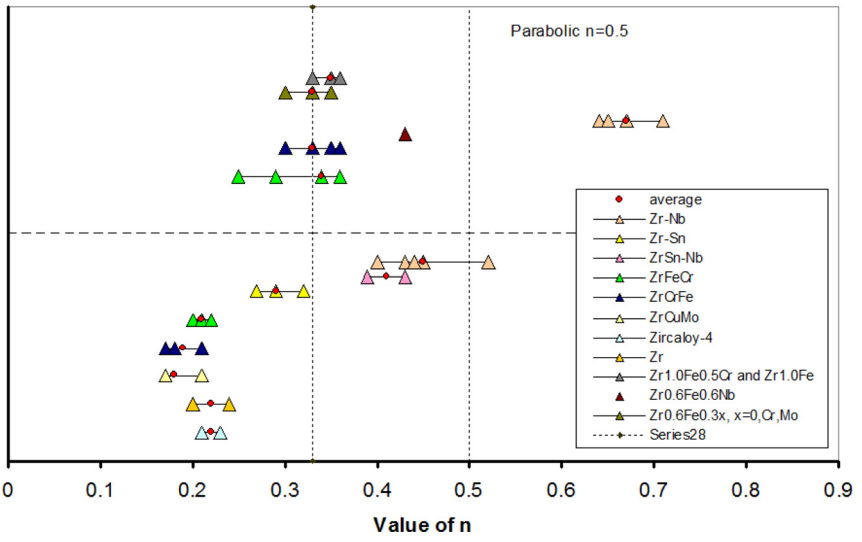

in the different oxide layer microstructures. Coincidentally, at that time the Advanced Photon Source (APS) at Argonne National Laboratory was being commissioned and scientists there developed a microbeam line that, using zone plate diffraction gratings, created a 0.2-μm beam [28]. This was a great advantage for

investigating a cross-section of the oxide structure in detail with a unique combination of elemental and phase sensitivity and spatial resolution. Initial experiments investigated precipitate size distribution and alloying element content in Zircaloys [29]. Fig. 8 shows the experimental setup at APS. By scanning the microbeam across the oxide thickness it was possible to acquire simultaneous diffraction and fluorescence information as a function of distance to the oxide/metal interface. This was done for oxides of various thicknesses and that were formed on different alloys [30].

By integrating the diffracted intensity along the angle χ (the angle along the diffraction line in Fig. 8), it was possible to obtain plots of diffraction intensity versus 2θ at each oxide location. By stacking those patterns sequentially, a complete picture of the oxide structure as a function of oxide depth is obtained. Fig. 9 shows one such plot in which the individual peaks corresponding to each phase are labeled. The metal and oxide layers are clearly visible, as is the periodicity of oxide formation, both in the monoclinic and tetragonal phases. A detailed oxide/metal interfacial structure was revealed, showing a suboxide phase (arrows) as well as a highly oriented tetragonal phase (see the 002t peak) that was observed in the slower growing oxides [31,32].

FIG. 8 Experimental setup for microbeam synchrotron radiation diffraction and fluorescence of oxide layers in zirconium alloys.

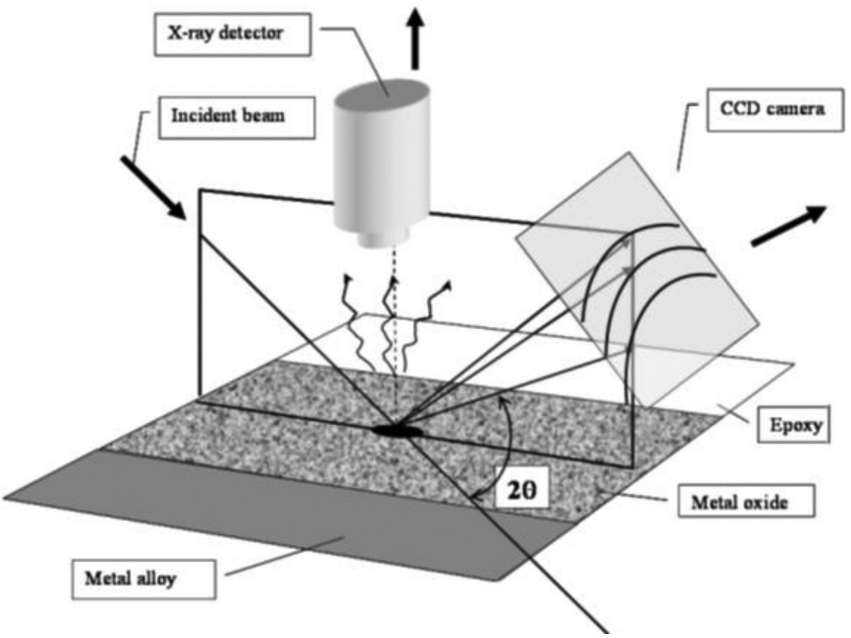

FIG. 9 X-ray–diffracted intensity versus 2θ angle scans from the oxide/metal to oxide/water interface in a ZIRLO oxide layer formed in 360°C water.

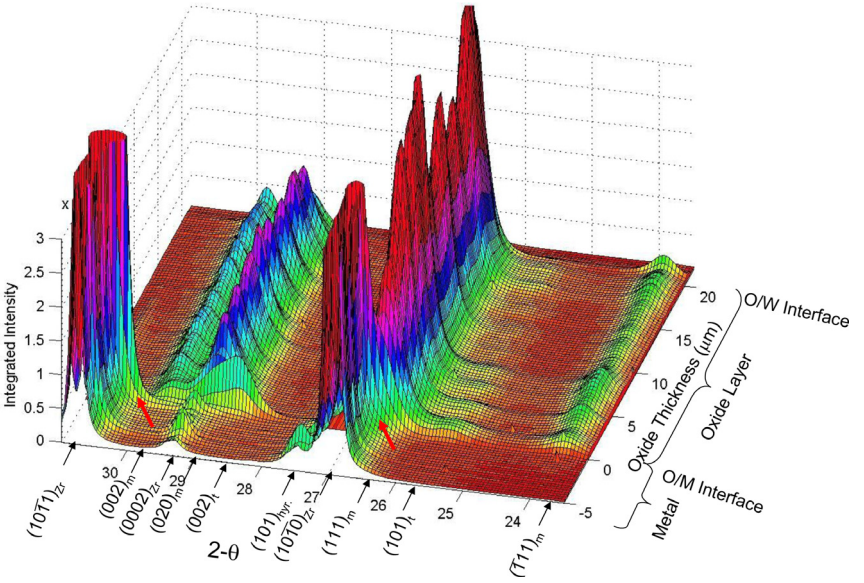

These observations were coupled with TEM [15] to discern in detail the oxide layer structure. More recent work that used atom probe tomography and electron energy loss spectroscopy coupled with TEM diffraction revealed the detailed nature of these suboxides that form ahead of the advancing oxide front [33–35].

Fig. 10 shows transmission electron micrographs of the oxide/metal interface of three different oxide layers along with the trace of the oxide grain boundaries. It was found that the more stable growing oxides exhibited larger and better aligned grains. It was also found that the tetragonal content scaled inversely with the onset of oxide transition; i.e., oxide layers with greater tetragonal content underwent earlier transitions.

The knowledge from detailed characterizations of the oxide layers performed using TEM and microbeam synchrotron radiation enabled us to propose a model for oxide growth [32]. According to this model, a high rate of oxide nucleation at the start of corrosion causes equiaxed grains to form, some of which are favorably oriented to grow in a columnar fashion with the column axis oriented along the 200 monoclinic direction (this designation according to [36]) because oxide growth in this direction minimizes stress accumulation. As the equiaxed grains grow beyond approximately 30 nm, the tetragonal oxide grains transform to monoclinic oxide. Once those monoclinic columns reach a length of approximately 200 nm, small misorientations cause the columns to stop growing and to have to re-nucleate. Since

FIG. 10 Grain size, shape, and orientation comparison near the oxide/metal interface of (a) Zircaloy-4, (b) ZIRLO, and (c) Zr-2.5Nb alloy oxides formed in 360°C pure water.

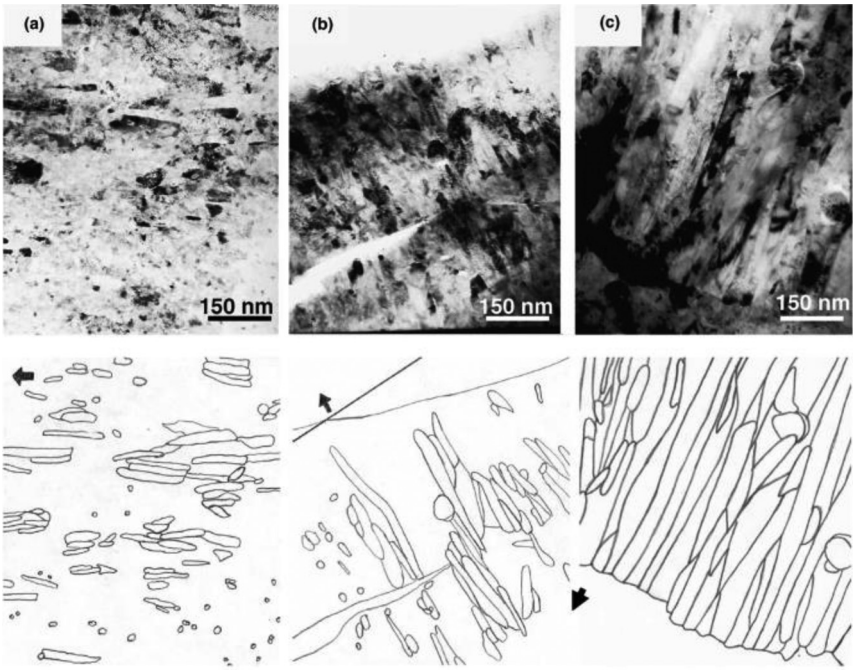

small grain size stabilizes the tetragonal phase, the tetragonal fraction is consistently higher near the oxide/metal interface (where small grains are constantly being formed) than in the bulk of the oxide. Once the in-plane stresses accumulate to a critical level, the oxide cracks horizontally (parallel to oxide metal interface), which causes the previously existing porosity to reach a percolation condition [24]. Once percolation occurs, water has access to the oxide/metal interface and increases the corrosion kinetics until the oxide reforms and the process continues. Recent observations of oxide microstructure during detailed TEM and APT examinations have been consistent with this model [33,35,37–42].

However, the most critical consequence of waterside corrosion is not the consumption of the cladding by the oxide or the deleterious impact of the oxide on cladding conductivity but rather the associated ingress of hydrogen. This leads to several issues that are discussed in the following sections.

Hydrogen

The ingress of hydrogen into the cladding during corrosion can severely affect cladding performance. Some of the principal mechanisms of fuel failure (cladding

failure) during longer reactor exposures are related to the formation of brittle hydrides and concomitant degradation of mechanical properties. The problem can be divided into three main areas of study:

- **Hydrogen pickup:** The pickup fraction (fraction of the hydrogen generated by the corrosion reaction that makes its way into the cladding) varies among alloys, with the corrosion environment and during the corrosion process.
- **Hydrogen transport:** Once the hydrogen enters the material, it redistributes in response to concentration gradients, temperature gradients, and stress gradients. Because hydrogen solubility varies strongly with temperature, localized precipitation of hydrides can occur.
- **Hydrogen embrittlement:** The precipitation of hydrides can decrease cladding ductility, especially if such hydrides precipitate in localized clusters such as hydride rims or blisters.

Each of the these topics is now discussed in turn.

HYDROGEN PICKUP

At the 15th Symposium on Zirconium in the Nuclear Industry, a study was presented of hydrogen pickup fraction as a function of corrosion time [43]. This was very interesting to our group because the Mechanistic Understanding of Zirconium Corrosion program in which we participated was scheduled to investigate the issue of hydrogen pickup. The hydrogen pickup fraction was often presented as being a constant for each alloy in a given environment, and clearly this was not the case in the data presented in this study.

To investigate this issue we corrosion tested several samples of various alloys and measured the corrosion kinetics in detail, as well as the hydrogen pickup. Because the measurement was to be done at short time intervals (and thus small hydrogen increments), it was necessary to find a technique that could measure hydrogen content with great precision. Such a technique was cold-neutron prompt gamma activation analysis, and through many back and forth trips between the National Institute of Standards and Technology and Westinghouse we measured the hydrogen contents of individual specimens as a function of oxide layer thickness during an autoclave corrosion test [44,45]. Fig. 11 shows the instantaneous hydrogen pickup fraction during autoclave corrosion of a ZIRLO sample. Also plotted in the figure is the corrosion weight gain showing the periodic kinetic transitions. Similar plots are also obtained for other alloys, including Zircaloy-4.

The precise hydrogen content measurements we obtained show that the instantaneous hydrogen pickup fraction varies in a consistent and periodic manner during the corrosion test, increasing just before the corrosion rate transition. Two facts are clear: (1) during the protective regime the hydrogen pickup fraction increases as the corrosion rate decreases, decreasing again just before the kinetic transition, and (2) the overall pickup fraction increases from one transition regime to the next. It turns out that this behavior can be generalized to many zirconium-based alloys [44]. Fig. 12 plots the total hydrogen picked up during corrosion against corrosion weight gain. In such a plot, a constant hydrogen pickup fraction would correspond

FIG. 11 Instantaneous hydrogen pickup fraction during corrosion of Zircaloy-4.

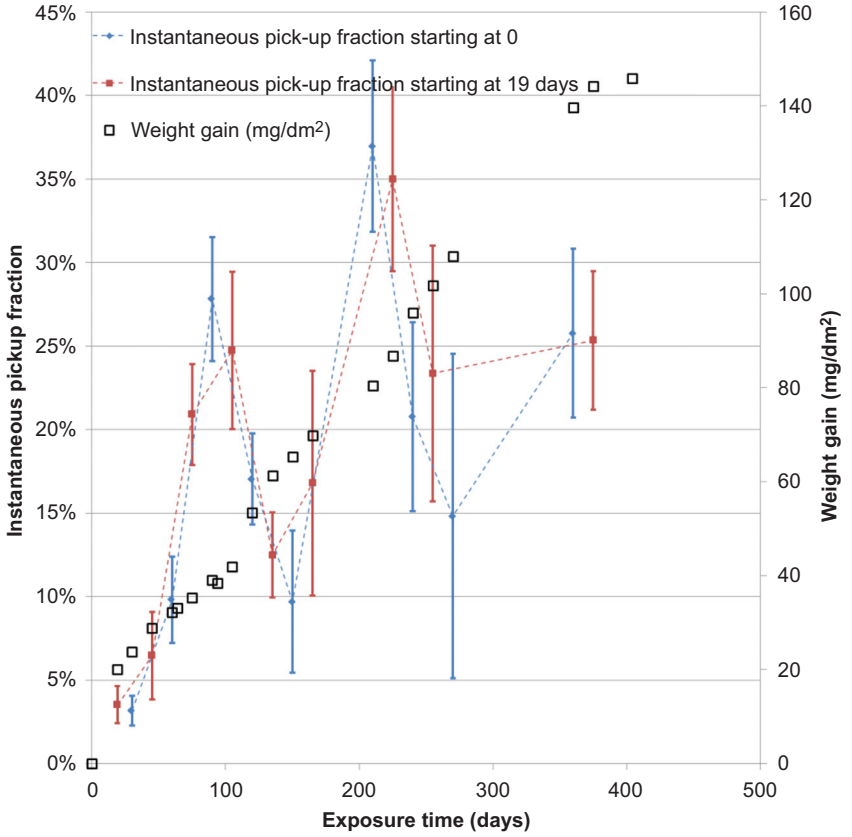

to a straight line. Straight lines corresponding to 10–40 % are plotted for reference. From the plot it is clear that for the alloys studied the hydrogen pickup fraction increases during corrosion and also from one transition period to the next. Further, Fig. 12 shows that the relative increases and pickup fractions are different for each alloy. These detailed measurements led to the hypothesis that hydrogen pickup is controlled by the oxide conductivity: the higher the oxide conductivity the lower the hydrogen pickup. This is because when the oxide conductivity is high, the corrosion reaction can be closed by electron transport through the oxide layer rather than by hydrogen ingress.

This hypothesis was later verified by in situ electrochemical impedance spectroscopy measurements that showed that as the oxide conductivity decreased, the hydrogen pickup increased as shown in Fig. 13 [46]. Previous micro-X-ray absorption near-edge structure (XANES) experiments had shown that such an evolution

FIG. 12 Total hydrogen pickup versus corrosion weight gain for four alloys during autoclave corrosion at 360°C.

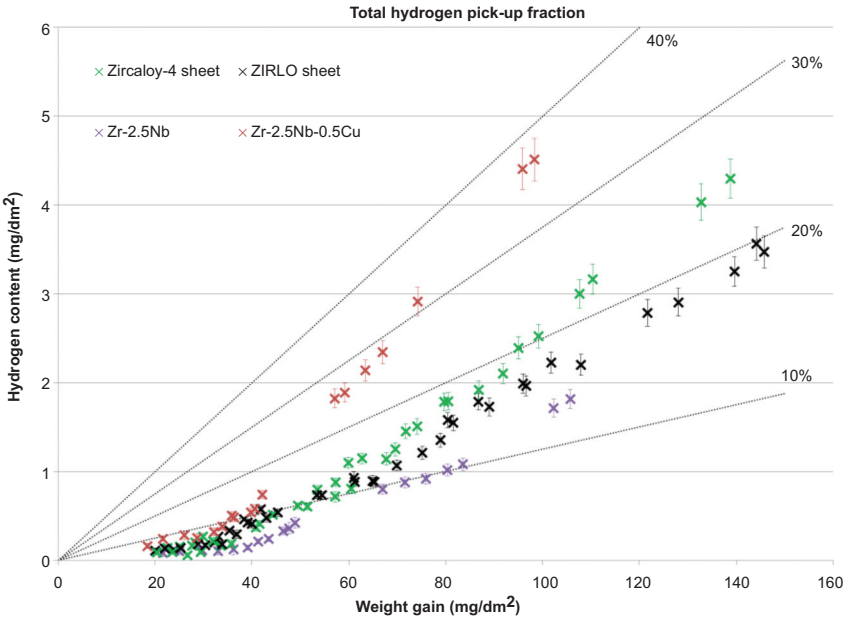

of protective oxide layer conductivity could be linked to the changing oxidation state of the alloying elements incorporated into the advancing oxide layer [46]. The XANES experiments showed that not only the alloying elements in precipitates but also the alloying elements in solid solution were found in metallic form near the oxide/metal interface and in oxidized form further away from it [44]. A related micro-XANES study of the oxidation state of nickel in high-burnup water rods showed that the presence of metallic nickel to a larger extent in the oxide layer in Zircaloy-2 could be responsible for its higher hydrogen pickup fraction [47].

This understanding of the processes of the coupling of the corrosion and hydrogen pickup was recently formalized into the C4 model [48]. This model is based on Fromhold's theory of a zero net current through the oxide [49]. Crucially, although the anode and cathode currents compensate one another, the concentrations of the two diffusing species, oxygen vacancies, and electrons do not necessarily compensate locally, creating a space charge in the protective oxide that affects the corrosion kinetics. In addition, the electric field so created causes the flux of oxygen ions (and thus the corrosion rate) to slow, which accounts for the lower values of n in the precipitate-bearing alloys as in those cases the oxide layer conductivity is low, resulting in sub-parabolic kinetics and creating a driving force for the ingress of hydrogen into the cladding. Those alloys then also show greater hydrogen pickup.

FIG. 13 Hydrogen pickup fraction versus oxide resistivity for Zircaloy 4 and ZIRLO at different stages of corrosion as measured by in situ **electrochemical impedance spectroscopy** [24].

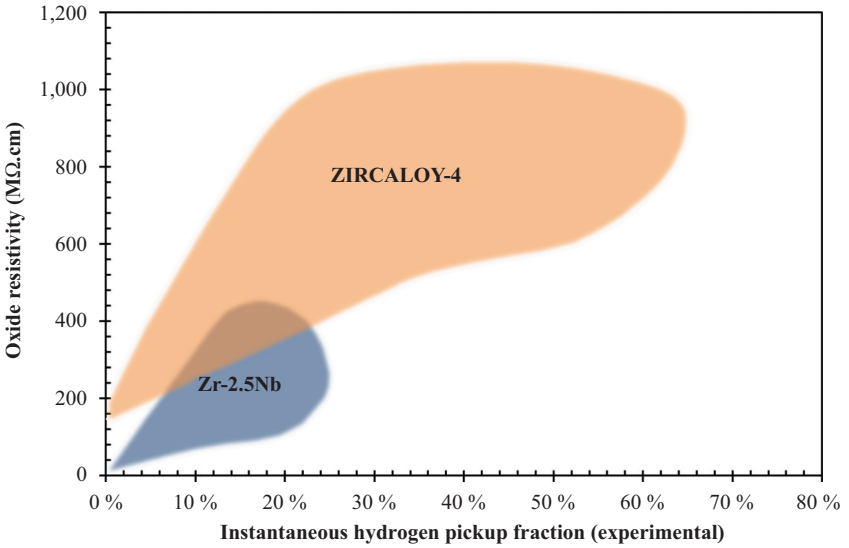

This model has the potential to explain the different corrosion kinetics and hydrogen pickup of the different alloys and of different precipitate morphologies. Work is ongoing to quantify the effect of precipitate morphology on oxide conductivity. The question can then be posed as to what happens to the hydrogen once it enters the cladding tube. This is discussed in the next section.

HYDROGEN TRANSPORT

Hydrogen is a very mobile atomic species in zirconium. It has a migration energy of 0.47 eV and as a result can respond very effectively not only to the well-known concentration gradients but also to imposed gradients in temperature or stress in the material. The temperature distribution in particular plays a crucial role, potentially causing the hydrogen distribution in the cladding tube to be inhomogeneous, which can happen in the radial, axial, and azimuthal directions. A radial temperature profile always exists in service because of the heat flux coming out of the fuel rod. For typical linear heat rates, a difference of 10–15 K is established between the inner and outer cladding surfaces. Axially, as the coolant temperature increases over the length of the fuel rod, the cladding temperature follows, but the gradient is small because the change occurs over a long distance. A more significant temperature gradient can occur between the mid- and inter-pellet regions, leading to hydrogen accumulation in the latter [50]. Finally, in the azimuthal direction, inhomogeneities in the flux and temperature distribution from an uneven neighborhood of fuel rods

create azimuthal temperature differences of the same order (10 K). In addition, the loss of thermal resistance from spalled oxide regions can cause temperature variations along the azimuth [51].

If one neglects smaller stress effects, hydrogen migration occurs as a result of Fick's Law and the Soret effect (temperature gradient creating a hydrogen flux) [50,52,53]. The hydrogen flux J_H is given by

$$J_H = -D_H \nabla C_H^{ss} - \frac{D_H C_H^{ss} Q^*}{RT^2} \nabla T \tag{5}$$

where:

D_H = diffusion coefficient of hydrogen in zirconium,
C_H^{SS} = space-dependent concentration of hydrogen in solid solution,
Q^* = heat of transport, and
T = temperature.

The first term on the right-hand side of Eq 5 represents the flux due to Fick's Law and the second, the flux resulting from the Soret effect. Eq 5 predicts that even in the absence of precipitation hydrogen will concentrate in the colder regions of the material.

HYDRIDE FORMATION

In addition to migration, once the terminal solid solubility is reached, hydrides will precipitate [54,55]. Note that two different and separate equations predict the terminal solid solubilities for precipitation (*TSSp*) and dissolution (*TSSd*) because a hysteresis exists between the two curves caused by the energy required for the nucleation of hydrides from solid solution.

Once nucleated, hydride growth can be described by Marino's model [56]:

$$\frac{dC_H^{ss}}{dt} = -\alpha^2 (C_H^{ss} - TSSp) \tag{6}$$

where:

α^2 = constant relating the hydrogen precipitation rate into hydrides to the hydrogen supersaturation in solid solution [57].

Kammenzind et al. [52] experimentally determined α^2, and this value was recently re-determined in an in situ examination of hydride precipitation with synchrotron radiation diffraction to be 4.5×10^{-4} s^{-1} in the temperature range studied [58]. A module was then developed for the BISON fuel performance code to predict hydrogen migration and precipitation under the conditions described previously [50].

Applying these well-known equations and using BISON in conjunction with solving the coupled heat transfer and neutron flux problem to find the temperature distribution in (r, θ, z) the hydrogen distribution in the fuel cladding tube after a certain time in service can be calculated. Detailed data from a CEA study on

hydrogen distribution determined during post-irradiation examination of rods after being discharged from service from the Gravelines plant and about which the power history, nearest-neighbor configurations were known [57] was made available to us. This allowed us to benchmark the model to predict the thickness of the hydride rim and the shape of the distribution of hydrogen in the radial direction [59]. **Fig. 14** shows the results of the calculation of hydrogen redistribution as a result of hydrogen flux from Fick's Law and the Soret effect and precipitation. Note that the simulation fully includes the cooldown schedule as the reactor shuts down.

The outer part of the cladding shown in **Fig. 14** corresponds to the rim of hydrides (very high hydrogen content) followed by two successive plateaus. Research is ongoing to explore this fertile field of investigation. As mentioned previously, the hydrides formed in the cladding have the potential to degrade cladding mechanical properties, and this is discussed in the following section.

HYDRIDE EMBRITTLEMENT

From the start of nuclear power it was recognized that in the case of a reactivity-initiated accident (RIA) the cladding needs to avoid catastrophic failure. If a control rod is ejected as a result, for example, of a failed control rod drive mechanism, a large insertion of reactivity could occur, leading to a very fast increase in the fission rate before getting turned around by the Doppler effect [60]. This abrupt increase in the fission rate causes a correspondingly fast (millisecond) increase in fuel

FIG. 14 Hydrogen content as a function of radial position for an irradiated rod, comparing post irradiation examination (PIE) and calculation.

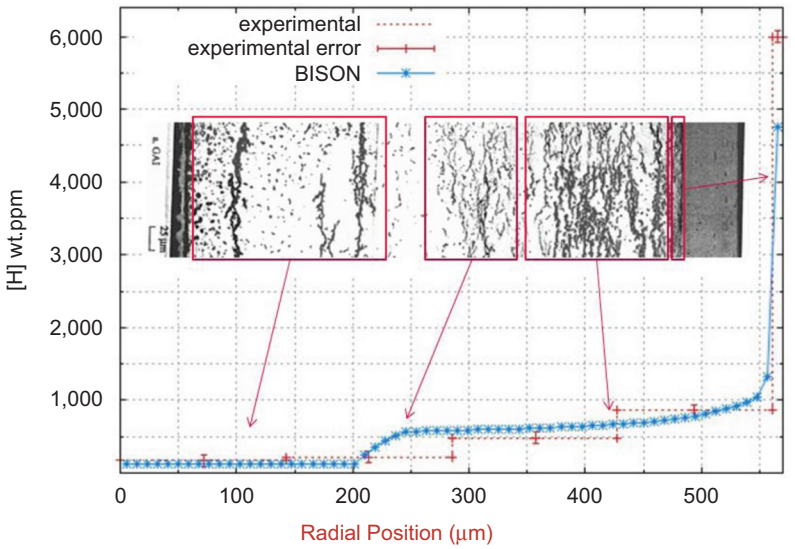

temperature. The fuel then expands against the cladding, causing it to deform at a very high strain rate (up to $10s^{-1}$). In that situation, the cladding needs to have some ductility to survive. To study cladding survivability in an RIA, MacDonald et al. [61] used the special power excursion reactor test (SPERT) and the power burst facility (PBF) test to examine fuel irradiated to up to 30 GWd/t and established limits for energy deposition that would cause cladding failure (180 cal/g) and cladding failure with fuel release (280 cal/g).

Our group at Penn State started to work on this problem as a result of the CABRI tests on irradiated fuel by which the resistance of higher-burnup fuel to an RIA was being evaluated [62]. In 1994, the CABRI-Rep-Na1 test showed brittle failure of cladding that had been irradiated to five cycles (67 GWd/t) and that showed a thick (greater than 80 μm) oxide layer with high hydrogen content (∼700 wt ppm) and with some spalled oxide. The approximate absorbed energy at failure was only 35 cal/g (much lower than the limits determined by MacDonald et al. [61]).

This generated an international effort to investigate the reason for such an abrupt loss of ductility. Since the embrittlement from radiation damage saturates relatively early during reactor exposure [63], the effort quickly focused on the role of hydrogen as the embrittling agent. It was necessary then to investigate the effects of high levels of hydrogen and inhomogeneous hydride distributions on cladding ductility. Crucially, the mechanical tests had to be performed using the correct strain path (through thickness crack propagation) and under the stress state thought to be prevalent during an RIA (between plane strain and equal biaxial tension depending on fuel/clad bonding) because it had been shown previously that the stress state had a strong influence on the failure of hydrided Zircaloy cladding [64].

In collaboration with Don Koss at Penn State, a sustained effort was developed to perform the proper tests to test the RIA susceptibility of hydrided cladding. A double-notch ring tensile test specimen was developed, now called the Penn State test, that deformed the material to failure under plane strain conditions in the center of the gage section [65]. The test was used to determine the ductility of hydrided cladding tubes under various hydrogen levels, at room temperature, and at high temperatures. **Fig. 15** shows the test geometry. The notches are oriented on top of the specimen, creating a self-similar deformation geometry. The gauge section has markings to determine the failure strain. Crucially, this sample geometry provides the correct strain path, which is through-thickness deformation and failure and thus a good representation of potential cladding failure. The results of the tests showed that both the hydrogen content and biaxial stress state reduced cladding ductility relative to the uniaxial testing of unhydrided cladding.

It was further recognized that the localization of hydrogen into hydride rims or blisters [66] discussed in the previous section could be much more deleterious to cladding ductility than a homogeneous distribution of hydrides would be. Accordingly, tests were conducted to measure the cladding ductility under plane strain deformation for a cladding with a hydride rim [67]. **Fig. 16** shows the variation of failure strain with rim thickness, indicating that the cladding has very little ductility

FIG. 15 The Penn State plane strain ring tensile test.

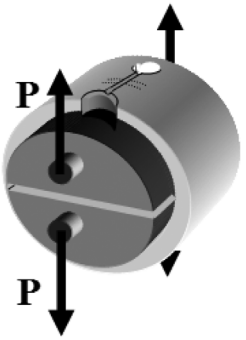

FIG. 16 Cladding ductility versus hydride layer thickness in hydrided Zircaloy-4.

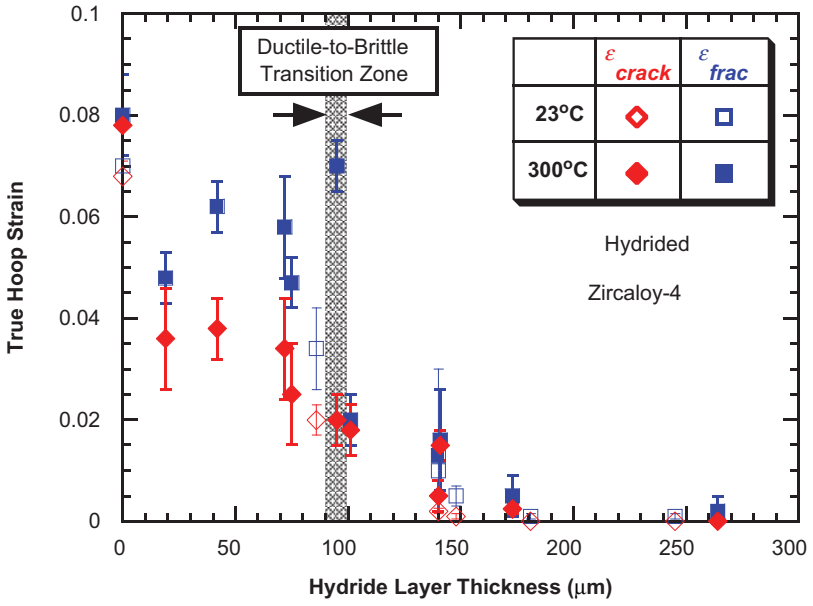

in the presence of a 100-μm-thick hydride layer. Other tests were developed to evaluate the cladding ductility in the presence of a deep lens-shaped hydride blister under plane strain and equal biaxial deformation. Pierron et al. [68] developed a flat sheet test to measure cladding ductility under plane strain deformation. A blister was artificially introduced by a special localized hydriding procedure. It was found

that for a given defect depth the cladding ductility was less affected by the presence of a blister than by the presence of a hydride rim, which makes sense because the blister has limited lateral extension to allow the crack to grow. A punch test developed by Glendening et al. [69] imposed equal biaxial deformation on a hydrided sheet that was then used to study the influence of blisters on cladding failure. By these tests and others recently reviewed in Desquines et al. [70], the effect of the stress state on the deformation and failure of hydrided cladding was quantified in terms of the reduction of the failure strain and change in the failure mode for different hydride distributions.

The Penn State test was later adapted to be used on irradiated material in the PROMETRA experimental testing program in France [71]. It was also used to test irradiated material in the Argonne test program [72,73].

Mechanical Properties

In addition to the measurement of ductility in the presence of hydride-induced defects, we were also interested in studying the influence of hydrogen on the deformation behavior of hydrided Zircaloy-4 [74]. The study showed little effect of the hydrogen content on either the strain or the strain-rate exponents of hydrided Zircaloy-4. The determination of the fracture toughness of Zircaloy is a topic of great interest, especially for crack propagation that follows the correct strain path, i.e., through the thickness of the sample. The variation of hydride microstructure (density, orientation) would be crucial parameters for determining the fracture toughness. To measure the fracture toughness of hydrided Zircaloy, a four-point bend test was used by Raynaud, Koss, and Motta [75] in conjunction with the creation of an artificial "linear blister" that upon initial deformation would inject a linear crack about the length of the sample and of controllable depth.

Combined with detailed quantitative metallography to characterize the hydride microstructure, this bend test was used to determine the fracture toughness of hydrided Zircaloy-4 as a function of hydride microstructure (in-plane, mixed, and out-of-plane hydrides) [75,76]. **Fig. 17** shows the propagation of a crack through the mixed population of hydride morphologies (sunburst and in-plane). The fracture toughness of the different regions was evaluated individually using this method.

This test pointed to the crucial role of hydride orientation in determining cladding failure. There was concern in the Used Fuel Disposition campaign of the DOE that the cladding material being taken out of the spent fuel pool to be put into dry storage could develop radial hydrides that would severely degrade cladding ductility and affect retrievability [77,78]. This could happen during the drying process in preparation for moving the fuel from the spent fuel pool to dry storage when the cladding is heated to drive moisture away and, in the process, dissolving a fraction of the hydrides. Because of the increased rod pressure at high temperatures the cooling occurs under a tensile hoop stress. It has been known since the 1960s that if

FIG. 17 Crack growth beyond a blister along hydrides during bend testing (a) propagation along sunburst hydrides and (b) crack tip blunting followed by secondary void formation.

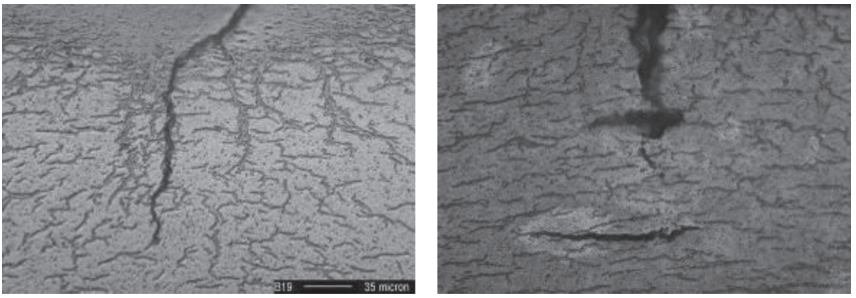

(a) (b)

one cools the cladding under a tensile hoop stress above a threshold stress radial (or out-of-plane) hydride platelets can form [79,80].

Accordingly a project was started that studied hydride dissolution and precipitation using synchrotron radiation diffraction [81–83]. Previous work had shown that the delta hydride phase is predominant [84]. Because the hydride precipitation could be achieved in situ under stress it was possible to reorient the hydrides during cooling. By monitoring during the test the intensity of the delta-111 hydride peak as the temperature increased, the hydride dissolution and precipitation temperatures were determined directly [81,82]. It was also possible to follow the increase in the zirconium matrix lattice parameter as hydrogen was dissolved into solid solution and its decrease when the hydrides precipitated, giving another window into the precipitation and dissolution behavior. By following instead the hydride lattice spacing along two different directions, a "hydride reorientation signature" was identified [83] (**Fig. 18**) as the difference in the full width at half maximum (FWHM) of the delta hydride peaks measured in two directions. For the reoriented hydride particles, the 111 planes parallel to the hydride face show a higher FWHM than the other.

The stress state present during cooling following the drying operation is expected to be biaxial rather than uniaxial. A project was launched at Penn State with Nuclear Regulatory Commission (NRC) funding to study hydride precipitation under biaxial stress. Test specimens were developed with a range of stress states. Testing showed that as biaxiality increases the threshold stress to reorient hydrides decreases significantly, as presented in this symposium [85]. **Fig. 19** shows that the threshold stress for hydride reorientation decreases by a factor of two between uniaxial and equal biaxial testing. This suggests that the testing for hydride reorientation during the preparation of cladding for used fuel disposition needs to be performed under higher biaxiality conditions than uniaxial tension.

FIG. 18 Hydride orientation and full width at half maximum of delta-111 hydride peak in the two directions. Transverse direction (TD) is the pulling direction.

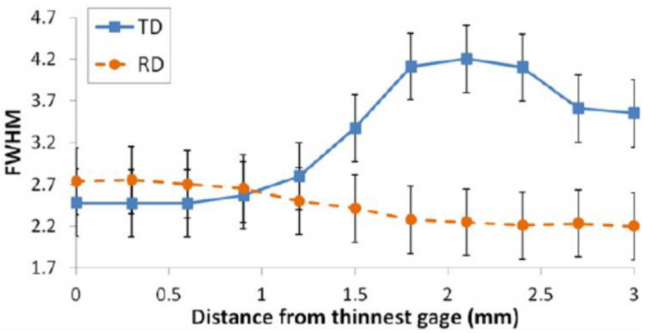

FIG. 19 Hydride threshold reorientation stress versus degree of biaxiality.

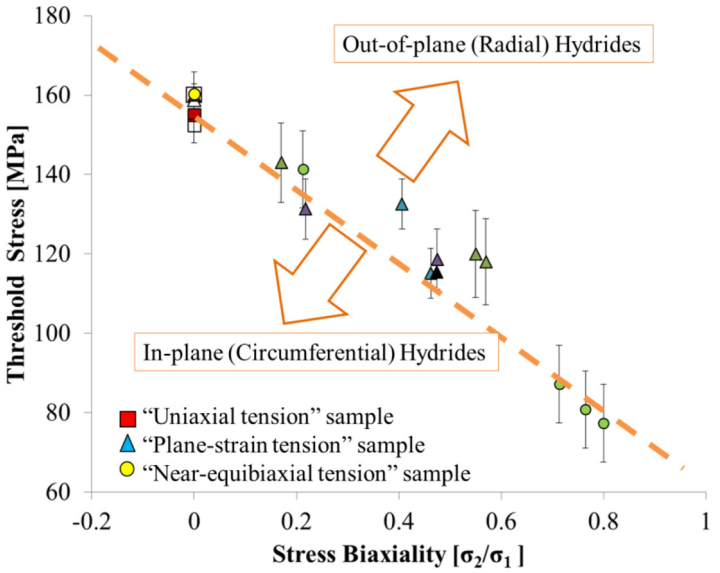

Perspectives

Although much progress has been made, much still remains to be understood concerning the behavior of zirconium cladding in reactors. The same can be said for any material that is subjected to the extreme environment of the reactor, especially in the more severe fuel duties currently being used by industry.

It is instructive to look at the similar perspectives written 20 years ago [63]. In that earlier review, C. Lemaignan and I suggested that greater knowledge of deformation mechanisms of zirconium alloy was needed, especially on the localization of deformation, which has certainly merited attention [86]. The connection of minor alloying elements on stabilizing <c>-component loops that contribute to irradiation growth has been shown to occur not only for iron [18] but also possibly for hydrogen [87]. Many studies have been developed and continue to be of detailed atomistic calculations of defect energetics that have informed detailed multiscale models [88,89].

In the review we also mentioned that the phase transformation associated with the oxide transition needed to be studied. Further study has shown no evidence that the tetragonal-to-monoclinic oxide transformation is connected to the oxide transition. In terms of corrosion, much mechanistic understanding has been achieved from the detailed characterization of the oxide microstructure and microchemistry and its relation to corrosion kinetics. Progress continues to be made in understanding oxide stability and the tendency to undergo breakaway corrosion [90]. This progress needs to continue to design better alloys.

From an overall perspective of analyzing fuel behavior in the core, recent advances in computing power have enabled even more detailed simulations of nuclear fuel performance. The multiphysics combination of materials behavior with neutron flux and thermal performance permits us to more accurately simulate fuel performance and gives us a better idea of the evolution of microstructure and material properties in these alloys. The recent development of fuel-performance codes such as BISON with more detailed underlying physics has the potential, once benchmarked, to lead to better predictive capabilities.

In terms of radiation damage, the specific role of irradiation on precipitate or solid-solution stability has not been completely resolved. The general problem of whether a particular microstructure or microchemistry is stable under irradiation is still an issue that merits further study. As well, the coupling between microstructure and microchemistry evolution during irradiation (e.g., hydrogen-enhancing loop formation, precipitates forming at extended sinks, segregation of solute to grain boundaries, etc.) is a particularly thorny problem that has been addressed only in an ad hoc manner. This could be in part because the best instruments to characterize defects (TEM) and microchemical changes (APT) can detect one characteristic well but the other less well. Newer transmission electron microscopes may provide a way forward. A greater ability to characterize, model, and understand the interactions between defects and material chemistry will be essential in predicting material behavior at high doses.

The process of hydride nucleation and precipitation and relative roles of microstructure, crystallographic texture, cooling rate, and sympathetic nucleation in promoting hydride precipitation along particular directions need to be understood because hydrides affect many fuel-failure processes in addition to those mentioned previously, such as delayed hydride cracking and secondary hydriding. Although considerable advances have certainly been made in understanding waterside

corrosion and hydrogen pickup, the specific role of alloying elements in the form of solid solution or precipitates—or specific distributions of precipitates—is not fundamentally understood, although a framework now exists for its comprehension.

Finally, in the wake of the Fukushima accident the development of zirconium-based accident-tolerant fuels (ATFs) is an area of active research. Although some of these ATFs are based on using materials such as SiC or FeCrAl, research is also ongoing on coating for zirconium-based alloys. Initial studies of the thermal and corrosion stability of ZIRLO with TiAlN multilayer coatings showed very good behavior and considerable reduction of corrosion [91].

Conclusions

A brief review was given of work performed by our group in the areas of radiation damage, corrosion, hydriding, and mechanical properties of zirconium alloys. An attempt was made to give the motivational and historical context in which the work was done as well as a summary of current problems. Much work continues to be needed in order to mechanistically understand the relevant phenomena and predict the performance of zirconium alloy nuclear fuel cladding with greater accuracy.

ACKNOWLEDGMENTS

The work described herein was achieved principally by my students over the last 25 years, with very important contributions from my collaborators, especially Don Koss at Penn State and Bob Comstock at Westinghouse. I thank both groups of individuals, from the bottom of my heart, for making this scientific career so rewarding to follow.

I am also very grateful to the people and institutions that hired me and gave me the opportunity to work (Don Olander at University of California, Berkeley, Clement Lemaignan at CEA-Grenoble, Rick Holt at AECL-Chalk River Laboratories, and Penn State University). Much of this work was accomplished using facilities at Argonne National Laboratory, including the IVEM and APS. Thanks are also due to the agencies that funded this work, including EPRI, CEA, AECL, NRC (Ralph Meyer and Harold Scott), NSF, Bettis Laboratories, and the DOE.

I owe the inspiration for a scientific career to my parents Anna Maria and Roberto, full professor in architecture at the Federal University of Rio de Janeiro, and to my grandfather, Arthur Moses, a former president of the Brazilian National Academy of Sciences. To them I owe a debt of gratitude that I will never be able to repay.

The love and support of my wife, Carol, and our children, Annie and Guilherme, has meant the world to me. I am overjoyed that they help me commemorate this recognition.

References

[1] Rickover, H. G., Geiger, L. D., and Lustman, B., "History of the Development of Zirconium Alloys for Use in Nuclear Reactors," Report No. TID-26740, Energy Research and Development Administration, Washington, DC, 1975.

[2] Lustman, B., "Zirconium Technology—Twenty Years of Evolution," *Zirconium in the Nuclear Industry, ASTM STP681*, J. H. Schemel and T. P. Papazoglou, Eds., ASTM International, Philadelphia, PA, 1979, pp. 5–54.

[3] Lustman, B. and Kerze, F., *The Metallurgy of Zirconium*, McGraw-Hill, New York, 1955.

[4] Kass, S., "The Development of the Zircaloys," *Corrosion of Zirconium Alloys, ASTM STP368*, W. Anderson, Ed., ASTM International, Philadelphia, PA, 1964, pp. 3–27.

[5] Jostsons, A., Kelly, P. M., Blake, R. G., and Farrell, K., "Neutron Irradiation Induced Defect Structures in Zirconium," *ASTM Special Technical Publication*, Vol. 683, 1979, pp. 46–61.

[6] Griffiths, M., "A Review of Microstructure Evolution in Zirconium Alloys during Irradiation," *J. Nucl. Mater.*, Vol. 159, 1988, pp. 190–218.

[7] Griffiths, M., "Evolution of Microstructure in hcp Metals during Irradiation," *J. Nucl. Mater.*, Vol. 205, 1993, pp. 225–241.

[8] Gilbert, R. W., Griffiths, M., and Carpenter, G. J. C., "Amorphous Intermetallics in Neutron Irradiated Zircaloys after High Fluences," *J. Nucl. Mater.*, Vol. 135, No. 2, 1985, pp. 265–268.

[9] Yang, W. J. S., Tucker, R. P., Cheng, B., and Adamson, R. B., "Precipitates in Zircaloy: Identification and the Effects of Irradiation and Thermal Treatment," *J. Nucl. Mater.*, Vol. 138, Nos. 2–3, 1986, pp. 185–195.

[10] Griffiths, M., Gilbert, R. W., and Carpenter, G. J. C., "Phase Instability, Decomposition and Redistribution of Intermetallic Precipitates in Zircaloy-2 and -4 during Neutron Irradiation," *J. Nucl. Mater.*, Vol. 150, No. 1, 1987, pp. 53–66.

[11] Oen, O. S., "Cross Sections for Atomic Displacements in Solids by Fast Electrons," ORNL-4897, Oak Ridge National Laboratory, Oak Ridge, Tennessee, 1973.

[12] Motta, A. T., Olander, D. R., and Machiels, A. J., "Electron-Irradiation Induced Amorphization of Precipitates in Zircaloy-2," *Effects of Radiation on Materials, ASTM STP1046*, N. H. Packan, R. E. Stoller, and A. S. Kumar, Eds., ASTM International, Philadelphia, PA, 1990, pp. 457–469.

[13] Motta, A. T., Lefebvre, F., and Lemaignan, C., "Amorphization of Precipitates in Zircaloy under Neutron, Ion and Electron Irradiation," *Zirconium in the Nuclear Industry, ASTM STP1132: 9th International Symposium*, C. M. Eucken and A. M. Garde, Eds., ASTM International, Philadelphia, PA, 1991, pp. 718–739.

[14] Motta, A. T. and Olander, D. R., "Theory of Electron-Irradiation-Induced Amorphization," *Acta Metall. Mater.*, Vol. 38, No. 11, 1990, pp. 2175–2185.

[15] Motta, A. T., Howe, L. M., and Okamoto, P. R., "Amorphization of Zr_3Fe under Electron Irradiation," *J. Nucl. Mater.*, Vol. 270, Nos. 1–2, 1999, pp. 174–186.

[16] Motta, A. T., "Amorphization of Intermetallic Compounds under Irradiation—A Review," *J. Nucl. Mater.*, Vol. 244, No. 3, 1997, pp. 227–250.

[17] Motta, A. T. and Lemaignan, C., "A Ballistic Mixing Model for the Amorphization of Precipitates in Zircaloy," *J. Nucl. Mater.*, Vol. 195, No. 3, 1992, pp. 277–285.

[18] de Carlan, Y., Regnard, C., Griffiths, M., Gilbon, D., and Lemaignan, C., "Influence of Iron in the Nucleation of ‹c› Component Dislocation Loops in Irradiated Zircaloy-4," *Zirconium in the Nuclear Industry: 11th International Symposium, ASTM STP1295*, E. R. Bradley and G. P. Sabol, Eds., ASTM International, West Conshohocken, PA, 1996, pp. 638–653.

[19] Zu, X. T., Sun, K., Atzmon, M., Wang, L. M., You, L. P., Wan, F. R., Busby, J. T., Was, G. S., and Adamson, R. B., "Effect of Proton and Ne Irradiation on the Microstructure of Zircaloy 4," *Philosoph. Mag.*, Vol. 85, Nos. 4–7, 2005, pp. 649–659.

[20] Garzarolli, F. and Stehle, H., "Behaviour of Structural Materials for Fuel and Control Elements in Light Water Cooled Power Reactors," *Improvements in Water Reactor Fuel Technology and Utilization*, IAEA, Vienna, Austria, pp. 387–407.

[21] Garzarolli, F., Steinberg, E., and Weidinger, H. G., "Microstructure and Corrosion Studies for Optimized PWR and BWR Zircaloy-Cladding," *Zirconium in the Nuclear Industry, ASTM STP1023: 8th International Symposium*, C. M. Eucken and L. F. P. Van Swam, Eds., ASTM International, Philadelphia, PA, 1989, pp. 202–212.

[22] Pécheur, D., Lefebvre, F., Motta, A. T., Lemaignan, C., and Charquet, D., "Oxidation of Intermetallic Precipitates in Zircaloy-4: Impact of Irradiation," *Zirconium in the Nuclear Industry, ASTM STP1245*, A. M. Garde and E. R. Bradley, Eds., ASTM International, West Conshohocken, PA, 1994, pp. 687–705.

[23] Pecheur, D., Lefebvre, F., Motta, A. T., Lemaignan, C., and Wadier, J.-F., "Precipitate Evolution in the Zircaloy-4 Oxide Layer," *J. Nucl. Mater.*, Vol. 189, No. 3, 1992, pp. 318–332.

[24] Motta, A. T., Couet, A., and Comstock, R. J., "Corrosion of Zirconium Alloys Used for Nuclear Fuel Cladding," *Ann. Rev. Mater. Res.*, Vol. 45, 2015, pp. 311–343.

[25] Motta, A. T., Gomes da Silva, M. J., Yilmazbayhan, A., Comstock, R. J., Cai, Z., and Lai, B., "Microstructural Characterization of Oxides Formed on Model Zr Alloys Using Synchrotron Radiation," *Zirconium in the Nuclear Industry, ASTM STP1505: 15th International Symposium*, B. Kammenzind and L. Magnus, Eds., ASTM International, West Conshohocken, PA, 2009, p. 486.

[26] Petigny, N., Barberis, P., Lemaignan, C., Valot, C., and Lallemant, M., "In Situ XRD Analysis of the Oxide Layers Formed by Oxidation at 743 K on Zircaloy-4 and Zr-1NbO," *J. Nucl. Mater.*, Vol. 280, No. 3, 2000, pp. 318–330.

[27] Li, H., Glavicic, H. M., and Spuznar, J. A., "A Model of Texture Formation in ZrO_2 Films," *Mater. Sci. Eng.*, Vol. A366, No. 1, 2004, pp. 164–174.

[28] Yun, W., Lai, B., Cai, Z., Maser, J., Legnini, D., and Gluskin, E., "Nanometer Focusing of Hard X-Rays by Phase Zone Plates," *Rev. Sci. Instrum.*, Vol. 70, No. 5, 1999, p. 2238.

[29] Motta, A. T., Erwin, K. T., Delaire, O., Birtcher, R. C., Chu, Y., Maser, J., Mancini, D. C., and Lai, B., "Synchrotron Radiation Study of Second-Phase Particles and Alloying Elements in Zirconium Alloys," *Zirconium in the Nuclear Industry: 13th International Symposium, ASTM STP1423*, G. D. Moan and P. Rudling, Eds., 2002, ASTM International, West Conshohocken, PA, 2002, pp. 59–77.

[30] Yilmazbayhan, A., Motta, A. T., Comstock, R. J., Sabol, G. P., Lai, B., and Cai, Z., "Structure of Zirconium Alloy Oxides Formed in Pure Water Studied with Synchrotron Radiation and Optical Microscopy: Relation to Corrosion Rate," *J. Nucl. Mater.*, Vol. 324, No. 1, 2004, pp. 6–22.

[31] Motta, A. T., Yilmazbayhan, A., Comstock, R. J., Partezana, J., Sabol, G. P., Lai, B., and Cai, Z., "Microstructure and Growth Mechanism of Oxide Layers Formed on Zr Alloys Studied with Micro-Beam Synchrotron Radiation," *Zirconium in the Nuclear Industry: 14th International Symposium, ASTM STP1467*, P. Rudling and B. Kammenzind, Eds., ASTM International, West Conshohocken, PA, 2005, pp. 205–232.

[32] Motta, A. T., Da Silva, M. J. G., Yilmazbayhan, A., Comstock, R. J., Cai, Z., and Lai, B., "Microstructural Characterization of Oxides Formed on Model Zr Alloys Using Synchrotron Radiation," *Zirconium in the Nuclear Industry: 15th International Symposium, ASTM STP1505*, B. Kammenzind and M. Limbäck, Eds., ASTM International, West Conshohocken, PA, 2009, pp. 486–506.

[33] de Gabory, B., Dong, Y., Motta, A. T., and Marquis, E. A., "EELS and Atom Probe Tomography Study of the Evolution of the Metal/Oxide Interface during Zirconium Alloy Oxidation," *J. Nucl. Mater.*, Vol. 462, 2015, pp. 304–309.

[34] Hudson, D., Ni, N., Lozano-Perez, S., Saxey, D., English, C., Smith, G. D. W., Sykes, J., and Grovenor, C., "The Atomic Scale Structure and Chemistry of the Zircaloy-4 Metal-Oxide Interface," presented at the *International Conference on Environmental Degradation of Materials in Nuclear Power Systems Water Reactors*, Virginia Beach, VA, August 23–27, 2009, American Nuclear Society, La Grange Park, IL, pp. 1407–1418.

[35] Dong, Y., Motta, A. T., and Marquis, E. A., "Atom Probe Tomography Study of Alloying Element Distributions in Zr Alloys and Their Oxides," *J. Nucl. Mater.*, Vol. 442, 2013, pp. 270–281.

[36] International Centre for Diffraction Data (ICDD), "Powder Diffraction File (PDF) Database: Card Nos. 37-1484 Monoclinic ZrO_2," ICDD, Newtown Square, PA.

[37] de Gabory, B. and Motta, A. T., "Structure of Zircaloy-4 Oxides Formed during Autoclave Corrosion," presented at *TopFuel 2013*, Charlotte, NC, September 15–19, 2013—unpublished.

[38] de Gabory, B., Motta, A. T., and Wang, K., "Transmission Electron Microscopy Characterization of Zircaloy-4 and ZIRLO™ Oxide Layers," *J. Nucl. Mater.*, Vol. 456, 2014, pp. 272–280.

[39] Ni, N., Hudson, D., Wei, J., Wang, P., Lozano-Perez, S., Smith, G. D. W., Sykes, J. M., Yardley, S. S., Moore, K. L., Lyon, S., Cottis, R., Preuss, M., and Grovenor, C. R. M., "How the Crystallography and Nanoscale Chemistry of the Metal/Oxide Interface Develops during the Aqueous Oxidation of Zirconium Cladding Alloys," *Acta Mater.*, Vol. 60, No. 20, 2012, pp. 7132–7149.

[40] Ni, N., Lozano-Perez, S., Jenkins, M. L., English, C., Smith, G. D. W., Sykes, J. M., and Grovener, C. R. M., "Porosity in Oxides on Zirconium Fuel Cladding Alloys, and Its Importance in Controlling Oxidation Rates," *Scripta Mater.*, Vol. 62, No. 8, 2010, pp. 564–567.

[41] Ni, N., Lozano-Perez, S., Sykes, J., and Grovenor, C., "Multi-Scale Characterisation of Oxide on Zirconium Alloys," *Mater. High Temp.*, Vol. 29, No. 3, 2012, pp. 166–170.

[42] Spengler, D. J., Motta, A. T., Bajaj, R., Seidensticker, J. R., and Cai, Z. H., "Characterization of Zircaloy-4 Corrosion Films Using Microbeam Synchrotron Radiation," *J. Nucl. Mater.*, Vol. 464, 2015, pp. 107–118.

[43] Harada, M. and Wakamatsu, R., "The Effect of Hydrogen on the Transition Behavior of the Corrosion Rate of Zirconium Alloys," *J. ASTM Int.*, Vol. 5, 2008, http://dx.doi.org/10.1520/JAI101117

[44] Couet, A., Motta, A. T., and Comstock, R. J., "Effect of Alloying Elements on Hydrogen Pickup in Zirconium Alloys," *Zirconium in the Nuclear Industry: 17th International Symposium, ASTM STP1543*, B. Comstock and P. Barbéris, Eds., ASTM International, West Conshohocken, PA, 2015, pp. 1–33.

[45] Couet, A., Motta, A. T., and Comstock, R. J., "Hydrogen Pickup Measurements in Zirconium Alloys: Relation to Oxidation Kinetics," *J. Nucl. Mater.*, Vol. 451, 2014, pp. 1–13.

[46] Couet, A., Motta, A. T., and Ambard, A., "Oxide Electronic Conductivity and Hydrogen Pickup Fraction in Zr Alloys," presented at *Transactions of the American Nuclear Society and Embedded Topical Meeting: Nuclear Fuels and Structural Materials for the Next Generation Nuclear Reactors*, Reno, NV, June 15–19, 2014, American Nuclear Society, La Grange, PA, 2014, pp. 845–848.

[47] Shivprasad, A. P., Motta, A. T., Kucuk, A., Yagnik, S., and Cai, Z., "Microbeam X-Ray Absorption Near-Edge Spectroscopy of Alloying Elements in the Oxide Layers of Irradiated Zircaloy-2," *Zirconium in the Nuclear Industry: 18th International Symposium, ASTM STP1597*, R. J. Comstock and A. T. Motta, Eds., ASTM International, West Conshohocken, PA, 2018, pp. 524–554.

[48] Couet, A., Motta, A. T., and Ambard, A., "The Coupled Current Charge Compensation Model for Zirconium Alloy Fuel Cladding Oxidation: I. Parabolic Oxidation of Zirconium Alloys," *Corrosion Sci.*, Vol. 100, 2015, pp. 73–84.

[49] Fromhold, A. T., *Theory of Metal Oxidation: Space Charge*, North Holland, Amsterdam, the Netherlands, 1980.

[50] Courty, O., Motta, A. T., and Hales, J. D., "Modeling and Simulation of Hydrogen Behavior in Zircaloy-4 Fuel Cladding," *J. Nucl. Mater.*, Vol. 452, Nos. 1–3, 2014, pp. 311–320.

[51] Mankosa, M. G., Piotrowski, C. J., Avramova, M. N., Motta, A. T., Ivanov, K. N., Stafford, S., and Williamson, R. L., "Anisotropic Azimuthal Power and Temperature Distribution as a Driving Force for Hydrogen Redistribution," *Proceedings of NURETH-16*, 2015, pp. 6229–6242.

[52] Kammenzind, B. F., Franklin, D. G., Peters, H. R., and Duffin, W. J., "Hydrogen Pickup and Redistribution in Alpha-Annealed Zircaloy-4," *Zirconium in the Nuclear Industry: 11th International Symposium, ASTM STP1295*, E. R. Bradley and G. P. Sabol, Eds., ASTM International, West Conshohocken, PA, 1996, pp. 338–370.

[53] Kammenzind, B. F., Berquist, B. M., Bajaj, R., Kreyns, P. H., and Franklin, D. G., "The Long-Range Migration of Hydrogen through Zircaloy in Response to Tensile and Compressive Stress Gradients," *Zirconium in the Nuclear Industry: 12th International Symposium, ASTM STP1354*, G. P. Sabol and G. D. Moan, Eds., ASTM International, West Conshohocken, PA, 2000, pp. 196–233.

[54] Kearns, J. J., "Terminal Solubility and Partitioning of Hydrogen in the Alpha Phase of Zirconium, Zircaloy-2 and Zircaloy-4," *J. Nucl. Mater.*, Vol. 22, No. 3, 1967, pp. 292–303.

[55] McMinn, A., Darby, E. C., and Schofield, J. S., "The Terminal Solid Solubility of Hydrogen in Zirconium Alloys," *Zirconium in the Nuclear Industry: 12th International Symposium, ASTM STP1354*, G. P. Sabol and G. D. Moan, Eds., ASTM International, West Conshohocken, PA, 2000, pp. 173–195.

[56] Marino, G. P., "Hydrogen Supercharging in Zircaloy," *Mater. Sci. and Eng.*, Vol. 7, No. 6, 1971, pp. 335–341.

[57] Zhang, J.-H., "Hydruration du Zircaloy-4 et Etude de la Distribution de l'Hydrogène dans une Gaine de Combustible REP," PhD thesis at Ecole Centrale-Paris and the Commissariat à l'Énergie Atomique, Paris, France, 1992.

[58] Courty, O. F., Motta, A. T., Piotrowski, C. J., and Almer, J. D., "Hydride Precipitation Kinetics in Zircaloy-4 Studied Using Synchrotron X-Ray Diffraction," *J. Nucl. Mater.*, Vol. 461, 2015, pp. 180–185.

[59] Lacroix, E. and Motta, A. T., "Validation of BISON Calculation of Hydrogen Distribution by Comparison to Experiment," presented at *TMS2016*, Nashville, TN, February 15–17, 2016, Minerals, Metals and Materials Society, Warrendale, PA, 2016, pp. 263–272.

[60] Meyer, R. O., McCardell, R. K., Chung, H. M., Diamond, D. J., and Scott, H. H., "A Regulatory Assessment of Test Data for Reactivity Initiated Accidents," *Nucl. Safety*, Vol. 37, No. 4, 1996, pp. 372–387.

[61] MacDonald, P. E., Seiffert, S. L., Martinson, Z. R., McCardell, R. K., Owen, D. E., and Fukuda, S. K., "Assessment of Light-Water-Reactor Fuel Damage during a Reactivity-Initiated Accident," *Nucl. Safety*, Vol. 21, No. 5, 1980, pp. 582–602.

[62] Papin, J., Balourdet, M., Lemoine, F., Lamare, F., Frizonnet, J. M., and Schmitz, F., "French Studies on High-Burnup Fuel Transient Behavior under RIA Conditions," *Nucl. Safety*, Vol. 37, 1996, pp. 289–327.

[63] Lemaignan, C. and Motta, A. T., "Zirconium Alloys in Nuclear Applications," *Materials Science and Technology: A Comprehensive Treatment*, Vol. 10 B, B. R. T. Frost, Ed., VCH, New York, 1994, pp. 1–51.

[64] Yunchang, F. and Koss, D. A., "The Influence of Multiaxial States of Stress on the Hydrogen Embrittlement of Zirconium Alloy Sheet," *Metall. Trans. A*, Vol. 16 A, No. 4, 1985, pp. 675–681.

[65] Link, T. M., Koss, D. A., and Motta, A. T., "Failure of Zircaloy Cladding under Transverse Plane-Strain Deformation," *Nucl. Eng. Des.*, Vol. 186, No. 3, 1998, pp. 379–394.

[66] Garde, A. M., Smith, G. P., and Pirek, R. C., "Effects of Hydride Precipitate Localization on the Ductility of Irradiated Zircaloy-4," *Zirconium in the Nuclear Industry: 11th International Symposium, ASTM STP1295*, E. R. Bradley and G. P. Sabol, Eds., ASTM International, West Conshohocken, PA, 1996, pp. 407–430.

[67] Daum, R. S., Bates, D. W., Koss, D. A., and Motta, A. T., "The Influence of a Hydrided Layer on the Fracture of Zircaloy-4 Cladding Tubes," presented at *Hydrogen Effects on Material Behaviour and Corrosion Deformation Interactions*, Moran, WY, September 22–26, 2002, Minerals, Metals and Materials Society, Warrendale, PA, 2003, pp. 249–258.

[68] Pierron, O. N., Koss, D. A., Motta, A. T., and Chan, K. S., "The Influence of Hydride Blisters on the Fracture of Zircaloy-4," *J. Nucl. Mater.*, Vol. 322, No. 1, 2003, pp. 21–35.

[69] Glendening, A., Koss, D. A., Pierron, O. N., Motta, A. T., and Daum, R. S., "Failure of Hydrided Zircaloy-4 under Equal-Biaxial and Plane-Strain Tensile Deformation," *J. ASTM Int.*, Vol. 2, 2005, http://dx.doi.org/10.1520/JAI12441

[70] Desquines, J., Koss, D. A., Motta, A. T., Cazalis, B., and Petit, M., "The Issue of Stress State during Mechanical Tests to Assess Cladding Performance during a Reactivity-Initiated Accident (RIA)," *J. Nucl. Mater.*, Vol. 412, No. 2, 2011, pp. 250–267.

[71] Cazalis, B., Desquines, J., Carassou, S., Le Jolu, T., and Bernaudat, C., "The Plane Strain Tests in the PROMETRA Program," *J. Nucl. Mater.*, Vol. 472, 2016, pp. 127–142.

[72] Daum, R. S., Majumdar, S., Bates, D. W., Motta, A. T., Koss, D. A., and Billone, M. C., "On the Embrittlement of Zircaloy-4 under RIA-Relevant Conditions," *Zirconium in the Nuclear Industry, ASTM STP1423*, G. D. Moan and P. Rudling, Eds., ASTM International, West Conshohocken, PA, 2002, pp. 702–718.

[73] Daum, R. S., Majumdar, S., and Billone, M. C., "Mechanical Properties of Irradiated Zircaloy-4 for Dry Cask Storage Conditions and Accidents," presented at the *Nuclear Safety Research Conference*, Washington, DC, October 20–22, 2003, U.S. Nuclear Regulatory Commission, Rockville, MD, 2004, pp. 85–96.

[74] Flanagan, M. E., Koss, D. A., and Motta, A. T., "The Influence of Hydrogen on the Deformation Behavior of Zircaloy-4," presented at the *Water Reactor Fuel Performance Meeting*, Seoul, Korea, October 19–22, 2008—unpublished.

[75] Raynaud, P. A., Koss, D. A., and Motta, A. T., "Crack Growth in the Through-Thickness Direction of Hydrided Thin-Wall Zircaloy Sheet," *J. Nucl. Mater.*, Vol. 420, Nos. 1–3, 2012, pp. 69–82.

[76] Raynaud, P. A., Motta, A., Koss, D. A., and Chan, K. S., "Fracture Toughness of Hydrided Zircaloy-4 Sheet under Through-Thickness Crack Growth Conditions," *Zirconium in the Nuclear Industry: 15th International Symposium, ASTM STP1505*, B. Kammenzind and M. Limbäck, Eds., ASTM International, West Conshohocken, PA, pp. 163–177.

[77] Aomi, M., Baba, T., Miyashita, T., Kamimura, K., Yasuda, T., Shinohara, Y., and Takeda, T., "Evaluation of Hydride Reorientation Behavior and Mechanical Properties for High-Burnup Fuel-Cladding Tubes in Interim Dry Storage," *J. ASTM Int.*, Vol. 5, No. 9, 2008, http://dx.doi.org/10.1520/JAI101262

[78] Daum, R. S., Majumdar, S., Liu, Y., and Billone, M. C., "Radial-Hydride Embrittlement of High-Burnup Zircaloy-4 Fuel Cladding," *J. Nucl. Sci. Tech.*, Vol. 43, No. 9, 2006, pp. 1054–1067.

[79] Ells, C. E., "The Stress Orientation of Hydride in Zirconium Alloys," *J. Nucl. Mater.*, Vol. 35, No. 3, 1970, pp. 306–315.

[80] Kearns, J. J., "Dissolution Kinetics of Hydride Platelets in Zircaloy-4," *J. Nucl. Mater.*, Vol. 27, No. 1, 1968, pp. 64–72.

[81] Colas, K., Motta, A., Daymond, M. R., and Almer, J., "Mechanisms of Hydride Reorientation in Zircaloy-4 Studied in Situ," *Zirconium in the Nuclear Industry: 17th International Symposium, ASTM STP1543*, B. Comstock and P. Barbéris, Eds., ASTM International, West Conshohocken, PA, 2013, pp. 1107–1137.

[82] Colas, K. B., Motta, A. T., Almer, J. D., Daymond, M. R., Kerr, M., Banchik, A. D., Vizcaino, P., and Santisteban, J. R., "In Situ Study of Hydride Precipitation Kinetics and Re-Orientation in Zircaloy Using Synchrotron Radiation," *Acta Mater.*, Vol. 58, No. 20, 2010, pp. 6575–6583.

[83] Colas, K. B., Motta, A. T., Daymond, M. R., and Almer, J. D., "Effect of Thermo-Mechanical Cycling on Zirconium Hydride Reorientation Studied in Situ with Synchrotron X-Ray Diffraction," *J. Nucl. Mater.*, Vol. 440, Nos. 1–3, 2013, pp. 586–595.

[84] Daum, R. S., Chu, Y. S., and Motta, A. T., "Identification and Quantification of Hydride Phases in Zircaloy-4 Cladding Using Synchrotron Radiation Diffraction," *J. Nucl. Mater.*, Vol. 392, No. 3, 2009, pp. 453–463.

[85] Cinbiz, M. N., Motta, A. T., Koss, D. A., and Billone, M., "Hydride Reorientation in Zircaloy-4 under Different States of Stress as Studied with in Situ X-Ray Diffraction," *Zirconium in the Nuclear Industry: 18th International Symposium, ASTM STP1597*, R. J. Comstock and A. T. Motta, Eds., ASTM International, West Conshohocken, PA, 2017, pp. 1252–1285.

[86] Onimus, F., Béchade, J.-L., Prioul, C., Pilvin, P., Monnet, I., Doriot, S., Verhaeghe, B., Gilbon, D., Robert, L., Legras, L., and Mardon, J.-P., "Plastic Deformation of Irradiated Zirconium Alloys: TEM Investigations and Micro-Mechanical Modeling," *Zirconium in the Nuclear Industry: 14th International Symposium, ASTM STP1467*, P. Rudling and B. Kammenzind, Eds., ASTM International, West Conshohocken, PA, 2005, pp. 53–78.

[87] Tournadre, L., Onimus, F., Béchade, J.-L., Gilbon, D., Cloue, J.-M., Mardon, J.-P., and Feaugas, X., "Impact of Hydrogen Pick-Up and Applied Stress on C-Component Loops: Toward a Better Understanding of the Radiation Induced Growth of Recrystallized Zirconium Alloys," *Zirconium in the Nuclear Industry: 17th International Symposium, ASTM STP1543*, B. Comstock and P. Barbéris, Eds., ASTM International, West Conshohocken, PA, 2015, pp. 853–894.

[88] Lumley, S. C., Murphy, S. T., Burr, P. A., Grimes, R. W., Chard-Tuckey, P. R., and Wenman, M. R., "The Stability of Alloying Additions in Zirconium," *J. Nucl. Mater.*, Vol. 437, Nos. 1–3, 2013, pp. 122–129.

[89] Domain, C. and Legris, A., "Ab Initio Atomic-Scale Determination of Point-Defect Structure in hcp Zirconium," *Philosoph. Mag.*, Vol. 85, Nos. 4–7, pp. 569–575, 2005.

[90] Ensor, B. M., Motta, A. T., Bajaj, R., Seidensticker, J. R., and Cai, Z., "XANES Analysis of Iron in Zircaloy-4 Oxides Formed at Different Temperatures Studied with Microbeam Synchrotron Radiation," *ANS LWR Fuel Performance Meeting, TopFuel 2015*, 2015, paper A0191.

[91] Alat, E., Motta, A. T., Comstock, R. J., Partezana, J. M., and Wolfe, D. E., "Ceramic Coating for Corrosion (c3) Resistance of Nuclear Fuel Cladding," *Surface Coatings Tech.*, Vol. 281, 2015, pp. 133–143.